

The effect of annealing on the nonlinear viscoelastic response of isotactic polypropylene

Aleksey D. Drozdov and Jesper deClaville Christiansen

Department of Production

Aalborg University

Fibigerstraede 16

DK-9220 Aalborg, Denmark

Abstract

Three series of tensile relaxation tests are performed on isotactic polypropylene at room temperature in the vicinity of the yield point. In the first series of experiments, injection-molded samples are used without thermal pre-treatment. In the second and third series, prior to testing the specimens are annealed at 130 °C for 4 and 24 hours, respectively.

Constitutive equations are derived for the time-dependent response of semicrystalline polymers at isothermal loading with small strains. A polymer is treated as an equivalent temporary network of macromolecules bridged by junctions (physical cross-links, entanglements and crystalline lamellae). Under loading, junctions slip with respect to their positions in the bulk material (which reflects the viscoplastic behavior), whereas chains separate from their junctions and merge with new ones at random times (which reflects the viscoelastic response). The network is thought of as an ensemble of meso-regions (MR) with various activation energies for detachment of chains from temporary nodes.

Adjustable parameters in the stress-strain relations are found by fitting observations. Experimental data demonstrate that the shape of the relaxation spectrum (characterized by the distribution of MRs with various potential energies) is independent of mechanical factors, but is altered at annealing. For specimens not subjected to thermal treatment, the growth of longitudinal strain does not affect the volume fraction of active MRs and the attempt rate for detachment of chains from their junctions. For annealed samples, the concentration of active MRs increases and the attempt rate decreases with strain. These changes in the time-dependent response are attributed to broadening of the distribution of strengths of crystalline lamellae at annealing.

1 Introduction

This paper is concerned with the influence of annealing at an elevated temperature on the nonlinear viscoelastic response of isotactic polypropylene (iPP) at room temperature. The objective of this study is three-fold:

1. to report experimental data in tensile relaxation tests on specimens annealed for various amounts of time at strains in the vicinity of the yield point,
2. to derive stress-strain relations for the nonlinear viscoelastic behavior of a semicrystalline polymer at isothermal uniaxial deformation,
3. to assess the effect of annealing on the time-dependent response of iPP in terms of the constitutive model.

Isotactic polypropylene is chosen for the analysis because of numerous applications of this polymer in industry (oriented films for packaging, reinforcing fibres, nonwoven fabrics, blends with thermoplastic elastomers, etc.). The goal of this study is to establish some correlations between mechanical properties, morphology and processing conditions (annealing at an elevated temperature) for injection-molded specimens. For a review of previous works on this subject, see [1] and the bibliography therein.

The nonlinear viscoelastic response of polypropylene was analyzed by Ward and Wolfe [2], see also [3], and Smart and Williams [4] three decades ago, and, more recently, by Ariyama [5, 6, 7, 8], Wortmann and Schulz [9, 10], Ibadon [11], Tomlins [12], Read and Tomlins [14, 15], Dutta and Edward [13] and Tomlins and Read [16].

The effect of physical aging (annealing at an elevated temperature followed by quench to ambient temperature) on the time-dependent behavior of PP was studied by Struik [17, 18], Chai and McCrum [19], Ibadon [11], Tomlins [12], Read and Tomlins [14, 15] and Tomlins and Read [16].

Dynamic mechanical analysis shows that the loss tangent of iPP demonstrates two pronounced maxima being plotted versus temperature [20, 21]. The first maximum (β -transition in the interval between $T = -20$ and $T = 10$ °C) is associated with the glass transition in the most mobile part of the amorphous phase, whereas the other maximum (α -transition in the interval between $T = 70$ and $T = 110$ °C) is attributed to the glass transition in the remaining part of the amorphous phase. This conclusion is confirmed by DSC (differential scanning calorimetry) traces for quenched PP that reveal an endotherm at $T = 70$ °C which can be ascribed to thermal activation of amorphous regions with restricted mobility under heating [21].

Isotactic polypropylene exhibits three different crystallographic forms: monoclinic α crystallites, (pseudo) hexagonal β structures, orthorhombic γ polymorphs, and “smectic” mesophase (arrays of chains with a better order in the longitudinal than in transverse chain direction). For a detailed review of iPP polymorphs, the reader is referred to the survey [22]. At rapid cooling of the melt (which is typical of injection molding), α crystallites and smectic mesophase are mainly developed, whereas metastable β and γ structures arise as minority components. Crystallization of β forms occurs either under stresses or with the help of β -nucleating agents added to the melt [23, 24]. Formation of γ polymorph requires high pressure for commercial grades of iPP, while it can be observed at atmospheric pressure in isotactic polypropylene with low molecular weight [25]. A unique feature of α structures in iPP is the lamellar crosshatching: development of transverse lamellae in spherulites that are oriented in the direction perpendicular to the direction of radial lamellae [26].

Scanning electron microscopy [27, 28], atomic force microscopy [29] and X-ray diffraction [21, 23, 24] reveal that in injection-molded specimens α spherulites have the characteristic size of the order of $100\ \mu\text{m}$ and they contain crystalline lamellae with thickness of 10 to 20 nm. The amorphous phase is located between spherulites and inside the spherulites between lamellae. It consists of (i) relatively mobile chains between spherulites and between radial lamellae inside spherulites, and (ii) severely restricted chains in the regions bounded by radial and tangential lamellae in α spherulites.

Annealing of injection-molded iPP at an elevated temperature results in (i) secondary crystallization of a part of the amorphous phase, (ii) thickening of radial lamellae, (iii) development of subsidiary lamellae, (iv) formation of lamellar superstructure, and (v) growth of the crystal perfection [30]. Other changes in the crystalline morphology of iPP driven by thermal treatment are the subject of debate. Some researchers [23, 24, 28, 29] conclude that the fraction of β spherulites increases at annealing in the interval of temperatures between 110 and $140\ ^\circ\text{C}$, which enhances ductility of iPP and improves its impact properties. According to other authors [21, 26, 31], annealing of iPP induces transformation of the smectic phase into monoclinic α spherulites without noticeable development of β polymorph.

Mechanical loading results in inter-lamellar separation, rotation and twist of lamellae, fine and coarse slip of lamellar blocks and their fragmentation [21]. Straining of iPP specimens causes chain slip through the crystals, sliding and breakage of tie chains and activation of restricted amorphous regions driven by lamellar disintegration. In the post-yield region, these changes in the micro-structure imply cavitation, breakage of crystallites, and formation of fibrils [32].

It is hard to believe that these morphological transformations in iPP can be adequately described by a constitutive model with a small number of adjustable parameters. To develop stress-strain relations, we apply a method of “homogenization of micro-structure” [33]. According to this approach, an equivalent phase is introduced whose deformation captures essential features of the response of a semicrystalline polymer with a complicated micro-structure. In this study, an amorphous phase is chosen as the equivalent phase because of the following reasons:

1. The viscoelastic response of semicrystalline polymers is conventionally associated with rearrangement of chains in amorphous regions [29].
2. Sliding of tie chains along and their detachment from lamellae play the key role in the time-dependent response of semicrystalline polymers [34, 35].
3. The viscoplastic flow in semicrystalline polymers is assumed to be “initiated in the amorphous phase before transitioning into the crystalline phase” [36].
4. Conventional models for polyethylene [33], polypropylene [37] and poly(ethylene terephthalate) [38] treat these polymers as networks of macromolecules.

Above the glass transition temperature for the mobile amorphous phase, isotactic polypropylene is thought of as a network of chains bridged by junctions. Deformation of a specimen induces slip of junctions with respect to their positions in the bulk material.

Sliding of junctions reflects slippage of tie molecules along lamellae and fine slip of lamellar blocks which are associated with the viscoplastic behavior of a semicrystalline polymer.

With reference to the concept of transient networks [39, 40, 41, 42], the viscoelastic response of iPP is modelled as separation of active chains from their junctions and attachment of dangling chains to temporary nodes. The network of macromolecules is assumed to be strongly inhomogeneous (this heterogeneity reflects the effect of spherulites on rearrangement of surrounding chains), and it is treated as an ensemble of meso-regions (MR) with various potential energies for detachment of active strands. Two types of MRs are distinguished: (i) active domains where strands separate from junctions as they are thermally agitated (these MRs model a mobile part of the amorphous phase), and (ii) passive domains where detachment of chains from junctions is prevented. Passive MRs are associated with a part of the amorphous phase whose mobility is restricted by (i) radial and tangential lamellae and (ii) surrounding macromolecules (because of density fluctuations in the amorphous phase).

Separation of active chains from temporary nodes is treated as a thermally-activated process whose rate obeys the Eyring equation [43] with a strain-dependent attempt rate. An increase in the relaxation rate of amorphous polymers at straining is conventionally attributed to the mechanically-induced growth of “free volume” between macromolecules which, in turn, implies an increase in their mobility [44, 45, 46].

Stretching of a specimen results in (i) a mechanically-induced changes in the rate of detachments of strands in active MRs and (ii) an increase in the concentration of active MRs. The latter is ascribed to (i) partial release of the amorphous phase in passive meso-domains driven by fragmentation of lamellae and (ii) breakage of van der Waals links between compactly packed chains in meso-domains with higher density.

The exposition is organized as follows. Section 2 is concerned with the description of the experimental procedure. Kinetic equations for sliding of junctions and reformation of active strands are developed in Section 3. Constitutive equations for uniaxial deformation are derived in Section 4. In Section 5 these relations are applied to fit experimental data. A brief discussion of our findings is presented in Section 6. Some concluding remarks are formulated in Section 7.

2 Experimental procedure

Isotactic polypropylene (Novolen 1100L) was supplied by BASF (Targor). ASTM dumbbell specimens were injection molded with length 14.8 mm, width 10 mm and height 3.8 mm. Three series of tests were performed. In the first series, the samples were used as received without thermal pre-treatment. In the second series, the specimens were annealed in an oven at the temperature 130 °C for 4 h and slowly cooled by air. In the third series of experiments, the specimens were annealed at the same temperature for 24 h and cooled by air.

Differential scanning calorimetry measurements were carried out on STA 449/Netzsch apparatus at the heating rate 5 K/min. The specimens with weight of about 15 mg were tested in Al₂O₃ pans covered by lid. The thermal analyzer was calibrated with 7 references ranging from In to Ni. The specific enthalpy of melting, ΔH_m , equals 86.9, 98.1 and 101.7

J/g, for non-annealed specimens, specimens annealed for 4 h, and specimens annealed for 24 h, respectively. With reference to [47], we accept the value 209 J/g as the enthalpy of fusion for a fully crystalline polypropylene. The degree of crystallinity, κ_c , is estimated as 41.6%, 46.8 % and 48.7 % for specimens not subjected to thermal treatment, samples annealed for 4 h, and specimens annealed for 24 h, respectively.

Although the degree of crystallinity changes rather weakly (but consistently) with an increase in the annealing time, the shape of DSC curves is noticeably altered in the interval of temperatures between 120 and 160 °C. DSC traces depicted in Figure 1 are similar to those found by other authors, see, e.g., [23, 26]. Labour et al. [23] attributed the growth of the low-temperature shoulder on the melting curve to the $\alpha \rightarrow \beta$ transition at annealing. According to Iijima and Strobl [26], the endothermal contribution on the low-temperature side of the DSC trace indicates the presence of α crystallites with varying stability.

Uniaxial tensile relaxation tests were performed at room temperature on a testing machine Instron-5568 equipped with electro-mechanical sensors for the control of longitudinal strains in the active zone of samples (the distance between clips was about 50 mm). The tensile force was measured by the standard loading cell. The engineering stress σ was determined as the ratio of the axial force to the cross-sectional area of the specimens in the stress-free state.

Any series of mechanical experiments included 9 relaxation tests at the longitudinal strains $\epsilon_1 = 0.02$, $\epsilon_2 = 0.04$, $\epsilon_3 = 0.06$, $\epsilon_4 = 0.08$, $\epsilon_5 = 0.10$, $\epsilon_6 = 0.12$, $\epsilon_7 = 0.14$, $\epsilon_8 = 0.16$, $\epsilon_9 = 0.18$, which corresponded to the domain of nonlinear viscoelasticity, sub-yield and post-yield regions for isotactic polypropylene (the yield strain, ϵ_y , was estimated by the supplier as 0.13). Mechanical tests were carried out at least one day after annealing of specimens to avoid the influence of physical aging on the time-dependent response of iPP.

Each relaxation test was performed on a new sample. No necking of specimens was observed in experiments (except for the test with $\epsilon_9 = 0.18$ on a specimen not subjected to thermal treatment, which was excluded from the consideration). In the k th relaxation test ($k = 1, \dots, 9$), a specimen was loaded with the cross-head speed 5 mm/min (that roughly corresponded to the strain rate $\dot{\epsilon}_0 = 0.05 \text{ min}^{-1}$) up to the longitudinal strain ϵ_k , which was preserved constant during the relaxation time $t_r = 20 \text{ min}$.

The engineering stresses, σ , at the beginning of the relaxation tests are plotted in Figure 2 together with the stress-strain curves for the specimens strained up to $\epsilon_9 = 0.18$. The figure demonstrates fair repeatability of experimental data.

Figure 2 shows that annealing for 4 h results in a pronounced increase in stress compared to virgin specimens. The growth of the annealing time implies a decrease in stress in the sub-yield region. The discrepancy between the stress-strain curves for specimens annealed for 4 and 24 h practically disappears in the post-yield domain.

Despite the coincidence of the stress-strain diagrams in the post-yield region for specimens annealed for 4 and 24 h, these samples demonstrate a noticeably different necking behavior. Necking of specimens not subjected to thermal pre-treatment occurs at the strain $\epsilon_n = 0.18$, necking of specimens annealed for 4 h takes place at the strain $\epsilon_n = 0.25$, whereas no necking is observed for specimens annealed for 24 h at stretching up to the strain $\epsilon = 0.30$.

The longitudinal stress, σ , is plotted versus the logarithm ($\log = \log_{10}$) of time t (the

initial instant $t = 0$ corresponds to the beginning of the relaxation process) in Figures 3 to 11. These figures demonstrate that the time of annealing strongly affects the shape of relaxation curves (especially, in the sub-yield region, see Figures 3 and 4). For any strain $\epsilon > 0.02$, stresses in the annealed specimens exceed those in the samples not subjected to thermal pre-treatment. In the sub-yield domain ($\epsilon < 0.1$) stresses in the specimens annealed for 4 h are higher than stresses in the samples annealed for 24 h.

Our aim now is to develop constitutive equations for the time-dependent behavior of a semicrystalline polymer to be employed for the quantitative analysis of these observations.

3 A micro-mechanical model

A semicrystalline polymer is treated as a temporary network of chains bridged by junctions. The network is modelled as an ensemble of meso-regions with various strengths of interaction between macromolecules. Two types of meso-domains are distinguished: passive and active. In passive MRs, inter-chain interaction prevents detachment of chains from junctions, which implies that all nodes in these domains are permanent. In active MRs, active strands (whose ends are connected to contiguous junctions) separate from the temporary junctions at random times when they are thermally agitated. An active chain whose end detaches from a junction is transformed into a dangling chain. A dangling chain returns into the active state when its free end captures a nearby junction at a random instant.

Denote by X the average number of active strands per unit mass of a polymer, by X_a the number of strands merged with the network in active MRs, and by X_p the number of strands connected to the network in passive MRs. Under stretching some crystalline lamellae (restricting mobility of chains in passive MRs) break, which results in a growth of the number of strands to be rearranged. As a consequence, the number of strands in active MRs increases and the number of strands in passive meso-domains decreases. This implies that the quantities X_a and X_p become functions of the current strain, ϵ , that obey the conservation law

$$X_a(\epsilon) + X_p(\epsilon) = X. \quad (1)$$

Rearrangement of strands in active MRs is thought of as a thermally activated process. The rate of detachment of active strands from their junctions in a MR with potential energy $\bar{\omega}$ in the stress-free state of a specimen is given by the Eyring equation [43]

$$\Gamma = \Gamma_a \exp\left(-\frac{\bar{\omega}}{k_B T}\right),$$

where k_B is Boltzmann's constant, T is the absolute temperature, and the pre-factor Γ_a is independent of energy $\bar{\omega}$ and temperature T . Introducing the dimensionless activation energy $\omega = \bar{\omega}/(k_B T_0)$, where T_0 is a reference temperature, and disregarding the effects of small increments of temperature, $\Delta T = T - T_0$, on the rate of separation, Γ , we arrive at the formula

$$\Gamma = \Gamma_a \exp(-\omega). \quad (2)$$

We suppose that Eq. (2) remains valid for an arbitrary loading process, provided that the attempt rate, Γ_a , is a function of the current strain, $\Gamma_a = \Gamma_a(\epsilon)$.

The distribution of active MRs with various potential energies is described by the probability density $p(\omega)$ that equals the ratio of the number, $N_a(\epsilon, \omega)$, of active meso-domains with energy ω to the total number of active MRs,

$$N_a(\epsilon, \omega) = X_a(\epsilon)p(\omega). \quad (3)$$

The distribution function for potential energies of active MRs, $p(\omega)$, is assumed to be strain-independent.

The ensemble of active meso-domains is described by the function $n_a(t, \tau, \omega)$ that equals the number of active strands at time t (per unit mass) belonging to active MRs with potential energy ω that have last been rearranged before instant $\tau \in [0, t]$. In particular, $n_a(0, 0, \omega)$ is the number (per unit mass) of active strands in active MRs with potential energy ω in a stress-free medium,

$$n_a(0, 0, \omega) = N_a(0, \omega), \quad (4)$$

and $n_a(t, t, \omega)$ is the number (per unit mass) of active strands in active MRs with potential energy ω in the deformed medium at time t (the initial time $t = 0$ corresponds to the instant when external loads are applied to the polymer),

$$n_a(t, t, \omega) = N_a(\epsilon(t), \omega). \quad (5)$$

The amount

$$\left. \frac{\partial n_a}{\partial \tau}(t, \tau, \omega) \right|_{t=\tau} d\tau$$

equals the number (per unit mass) of dangling strands in active MRs with potential energy ω that merge with the network within the interval $[\tau, \tau + d\tau]$, and the quantity

$$\frac{\partial n_a}{\partial \tau}(t, \tau, \omega) d\tau$$

is the number of there strands that have not detached from temporary junctions during the interval $[\tau, t]$. The number (per unit mass) of strands in active MRs that separate (for the first time) from the network within the interval $[t, t + dt]$ reads

$$-\frac{\partial n_a}{\partial t}(t, 0, \omega) dt,$$

whereas the number (per unit mass) of strands in active MRs that merged with the network during the interval $[\tau, \tau + d\tau]$ and, afterwards, separate from the network within the interval $[t, t + dt]$ is given by

$$-\frac{\partial^2 n_a}{\partial t \partial \tau}(t, \tau, \omega) dt d\tau.$$

The rate of detachment, Γ , equals the ratio of the number of active strands that separate from the network per unit time to the current number of active strands. Applying this

definition to active strands that merged with the network during the interval $[\tau, \tau + d\tau]$ and separate from temporary junctions within the interval $[t, t + dt]$, we find that

$$\frac{\partial^2 n_a}{\partial t \partial \tau}(t, \tau, \omega) = -\Gamma(\epsilon(t), \omega) \frac{\partial n_a}{\partial \tau}(t, \tau, \omega). \quad (6)$$

Changes in the function $n_a(t, 0, \omega)$ are governed by two processes at the micro-level: (i) detachment of active strands from temporary nodes, and (ii) mechanically-induced activation of passive MRs. The kinetic equation for this function reads

$$\frac{\partial n_a}{\partial t}(t, 0, \omega) = -\Gamma(\epsilon(t), \omega) n_a(t, 0, \omega) + \frac{\partial N_a}{\partial \epsilon}(\epsilon(t), \omega) \frac{d\epsilon}{dt}(t). \quad (7)$$

The solution of Eq. (7) with initial condition (4) is given by

$$\begin{aligned} n_a(t, 0, \omega) &= N_a(0, \omega) \exp\left[-\int_0^t \Gamma(\epsilon(s), \omega) ds\right] \\ &+ \int_0^t \frac{\partial N_a}{\partial \epsilon}(\epsilon(\tau), \omega) \frac{d\epsilon}{dt}(\tau) \exp\left[-\int_\tau^t \Gamma(\epsilon(s), \omega) ds\right] d\tau. \end{aligned} \quad (8)$$

It follows from Eq. (6) that

$$\frac{\partial n_a}{\partial \tau}(t, \tau, \omega) = \varphi(\tau, \omega) \exp\left[-\int_\tau^t \Gamma(\epsilon(s), \omega) ds\right], \quad (9)$$

where

$$\varphi(\tau, \omega) = \left. \frac{\partial n_a}{\partial \tau}(t, \tau, \omega) \right|_{t=\tau}. \quad (10)$$

To determine the function $\varphi(t, \omega)$, we use the identity

$$n_a(t, t, \omega) = n_a(t, 0, \omega) + \int_0^t \frac{\partial n_a}{\partial \tau}(t, \tau, \omega) d\tau. \quad (11)$$

Equations (5) and (11) imply that

$$n_a(t, 0, \omega) + \int_0^t \frac{\partial n_a}{\partial \tau}(t, \tau, \omega) d\tau = N_a(\epsilon(t), \omega). \quad (12)$$

Differentiating Eq. (12) with respect to time and using Eq. (10), we obtain

$$\varphi(t, \omega) + \frac{\partial n_a}{\partial t}(t, 0, \omega) + \int_0^t \frac{\partial^2 n_a}{\partial t \partial \tau}(t, \tau, \omega) d\tau = \frac{\partial N_a}{\partial \epsilon}(\epsilon(t), \omega) \frac{d\epsilon}{dt}(t).$$

This equality together with Eqs. (6), (7) and (11) results in

$$\varphi(t, \omega) = \Gamma(\epsilon(t), \omega) n_a(t, t, \omega). \quad (13)$$

Substituting expression (13) into Eq. (9) and using Eq. (5), we arrive at the formula

$$\frac{\partial n_a}{\partial \tau}(t, \tau, \omega) = \Gamma(\epsilon(t), \omega) N_a(\epsilon(t), \omega) \exp\left[-\int_\tau^t \Gamma(\epsilon(s), \omega) ds\right]. \quad (14)$$

The kinetics of rearrangement of strands in active MRs is described by Eqs. (2), (3), (8) and (14). These relations are determined by (i) the distribution function $p(\omega)$ for active MRs with various potential energies ω , (ii) the function $\Gamma_a(\epsilon)$ that characterizes the effect of strains on the attempt rate, and (iii) the function

$$\kappa_a(\epsilon) = \frac{X_a(\epsilon)}{X}, \quad (15)$$

that reflects mechanically-induced activation of passive MRs.

Rearrangement of strands in active MRs reflects the viscoelastic response of a semicrystalline polymer. The viscoplastic behavior is associated with the mechanically-induced slippage of junctions with respect to their positions in the bulk material.

Denote by $\epsilon_u(t)$ the average strain induced by sliding of junctions between macromolecules (the subscript index “u” means that $\epsilon_u(t)$ coincides with the residual strain in a specimen which is suddenly unloaded at instant t). The elastic strain (that reflects elongation of active strands in a network) is denoted by $\epsilon_e(t)$. The strains $\epsilon_e(t)$ and $\epsilon_u(t)$ are connected with the macro-strain $\epsilon(t)$ by the conventional formula

$$\epsilon(t) = \epsilon_e(t) + \epsilon_u(t). \quad (16)$$

We adopt the first order kinetics for slippage of junctions with respect to the bulk material, which implies that the increment of the viscoplastic strain, $d\epsilon_u$, induced by the growth of the macro-strain, ϵ , by an increment, $d\epsilon$, is proportional to the absolute value of the stress σ ,

$$\frac{d\epsilon_u}{d\epsilon} = B|\sigma| \operatorname{sign}\left(\sigma \frac{d\epsilon}{dt}\right), \quad (17)$$

where the pre-factor B is a non-negative function of stress, strain and the strain rate,

$$B = B\left(\sigma, \epsilon, \frac{d\epsilon}{dt}\right).$$

The last multiplier in Eq. (17) determines the direction of the viscoplastic flow of junctions. Equation (17) is presented in the form

$$\frac{d\epsilon_u}{dt}(t) = B\left(\sigma(t), \epsilon(t), \frac{d\epsilon}{dt}\right) |\sigma(t)| \operatorname{sign}\left[\sigma(t) \frac{d\epsilon}{dt}(t)\right] \frac{d\epsilon}{dt}(t), \quad \epsilon_u(0) = 0, \quad (18)$$

which implies that the rate of sliding vanishes when the macro-strain, ϵ , remains constant.

4 Constitutive equations

An active strand is modelled as a linear elastic solid with the mechanical energy

$$w(t) = \frac{1}{2} \mu e^2(t),$$

where μ is the average rigidity per strand and e is the strain from the stress-free state to the deformed state.

For strands belonging to passive meso-domains, the strain e coincides with ϵ_e . Multiplying the strain energy per strand by the number of strands in passive MRs, we find the mechanical energy of meso-domains where rearrangement of chains is prevented by surrounding lamellae,

$$W_p(t) = \frac{1}{2}\mu X_p(\epsilon(t))\epsilon_e^2(t). \quad (19)$$

With reference to the conventional theory of temporary networks [42], we assume that stresses in dangling strands totally relax before these strands merge with the network. This implies that the reference (stress-free) state of a strand that is attached to the network at time τ coincides with the deformed state of the network at that instant. For active strands that have not been rearranged until time t , the strain $e(t)$ coincides with $\epsilon_e(t)$, whereas for active strands that have last been merged with the network at time $\tau \in [0, t]$, the strain $e(t, \tau)$ is given by

$$e(t, \tau) = \epsilon_e(t) - \epsilon_e(\tau).$$

Summing the mechanical energies of active strands belonging to active MRs with various potential energies, ω , that were rearranged at various instants, τ , we find the mechanical energy of active meso-domains,

$$W_a(t) = \frac{1}{2}\mu \int_0^\infty d\omega \left\{ n_a(t, 0, \omega) \epsilon_e^2(t) + \int_0^t \frac{\partial n_a}{\partial \tau}(t, \tau, \omega) [\epsilon_e(t) - \epsilon_e(\tau)]^2 d\tau \right\}. \quad (20)$$

The mechanical energy per unit mass of a polymer reads $W(t) = W_a(t) + W_p(t)$. Substituting expressions (19) and (20) into this equality and using Eq. (16), we arrive at the formula

$$\begin{aligned} W(t) = & \frac{1}{2}\mu \left\{ X_p(\epsilon(t)) (\epsilon(t) - \epsilon_u(t))^2 + \int_0^\infty d\omega \left[n_a(t, 0, \omega) (\epsilon(t) - \epsilon_u(t))^2 \right. \right. \\ & \left. \left. + \int_0^t \frac{\partial n_a}{\partial \tau}(t, \tau, \omega) \left((\epsilon(t) - \epsilon_u(t)) - (\epsilon(\tau) - \epsilon_u(\tau)) \right)^2 d\tau \right] \right\}. \end{aligned} \quad (21)$$

Differentiation of Eq. (21) with respect to time results in

$$\frac{dW}{dt}(t) = \mu \left[A(t) \frac{d\epsilon}{dt}(t) - \frac{1}{2} (A_1(t) + A_2(t)) \right], \quad (22)$$

where

$$\begin{aligned} A(t) &= X_p(\epsilon(t)) [\epsilon(t) - \epsilon_u(t)] + \int_0^\infty d\omega \left\{ n_a(t, 0, \omega) [\epsilon(t) - \epsilon_u(t)] \right. \\ &\quad \left. + \int_0^t \frac{\partial n_a}{\partial \tau}(t, \tau, \omega) [(\epsilon(t) - \epsilon_u(t)) - (\epsilon(\tau) - \epsilon_u(\tau))] d\tau \right\}, \\ A_1(t) &= -\frac{\partial X_p}{\partial \epsilon}(\epsilon(t)) \frac{d\epsilon}{dt}(t) [\epsilon(t) - \epsilon_u(t)]^2 - \int_0^\infty d\omega \left\{ \frac{\partial n_a}{\partial t}(t, 0, \omega) [\epsilon(t) - \epsilon_u(t)]^2 \right. \\ &\quad \left. + \int_0^t \frac{\partial^2 n_a}{\partial t \partial \tau}(t, \tau, \omega) [(\epsilon(t) - \epsilon_u(t)) - (\epsilon(\tau) - \epsilon_u(\tau))]^2 d\tau \right\}, \\ A_2(t) &= 2A(t) \frac{d\epsilon_u}{dt}(t). \end{aligned} \quad (23)$$

Bearing in mind Eqs. (1), (3), (5) and (11), we transform the first equality in Eq. (23) as follows:

$$A(t) = X[\epsilon(t) - \epsilon_u(t)] - \int_0^\infty d\omega \int_0^t \frac{\partial n_a}{\partial \tau}(t, \tau, \omega) [\epsilon(\tau) - \epsilon_u(\tau)] d\tau. \quad (24)$$

Substitution of expressions (1), (3), (6) and (7) into the second equality in Eq. (23) yields

$$\begin{aligned} A_1(t) = & \int_0^\infty \Gamma(\epsilon(t), \omega) d\omega \left\{ n_a(t, 0, \omega) [\epsilon(t) - \epsilon_u(t)]^2 \right. \\ & \left. + \int_0^t \frac{\partial n_a}{\partial \tau}(t, \tau, \omega) [(\epsilon(t) - \epsilon_u(t)) - (\epsilon(\tau) - \epsilon_u(\tau))]^2 d\tau \right\}. \end{aligned} \quad (25)$$

For uniaxial loading with small strains at the reference temperature T_0 , the Clausius-Duhem inequality reads

$$T_0 Q(t) = -\frac{dW}{dt}(t) + \frac{1}{\rho} \sigma(t) \frac{d\epsilon}{dt}(t) \geq 0,$$

where ρ is mass density, and Q is the rate of entropy production per unit mass. Substitution of expression (22) into this equation implies that

$$T_0 Q(t) = \frac{1}{\rho} [\sigma(t) - \rho \mu A(t)] \frac{d\epsilon}{dt}(t) + \frac{1}{2} [A_1(t) + A_2(t)] \geq 0. \quad (26)$$

Because Eq. (26) is to be fulfilled for an arbitrary program of straining, $\epsilon = \epsilon(t)$, the expression in the first square brackets vanishes. This assertion together with Eq. (24) results in the stress-strain relation

$$\sigma(t) = E \left\{ [\epsilon(t) - \epsilon_u(t)] - \frac{1}{X} \int_0^\infty d\omega \int_0^t \frac{\partial n_a}{\partial \tau}(t, \tau, \omega) [\epsilon(\tau) - \epsilon_u(\tau)] d\tau \right\}, \quad (27)$$

where $E = \rho \mu X$ is an analog of the Young modulus. It follows from Eqs. (18), (23), (24) and (27) that

$$A_2(t) = \frac{2}{\rho \mu} B(\sigma(t), \epsilon(t), \frac{d\epsilon}{dt}(t)) \sigma^2(t) \left| \frac{d\epsilon}{dt}(t) \right|. \quad (28)$$

According to Eqs. (25) and (28), the functions $A_1(t)$ and $A_2(t)$ are non-negative for an arbitrary program of loading, which implies that the Clausius-Duhem inequality (26) is satisfied.

Substitution of Eqs. (3), (14) and (15) into Eq. (27) results in the constitutive equation

$$\begin{aligned} \sigma(t) = & E \left\{ [\epsilon(t) - \epsilon_u(t)] - \kappa_a(\epsilon(t)) \int_0^\infty p(\omega) d\omega \right. \\ & \left. \times \int_0^t \Gamma(\epsilon(t), \omega) \exp \left[- \int_\tau^t \Gamma(\epsilon(s), \omega) ds \right] [\epsilon(\tau) - \epsilon_u(\tau)] d\tau \right\}. \end{aligned} \quad (29)$$

Given functions $p(\omega)$, $\Gamma_a(\epsilon)$ and $\kappa_a(\epsilon)$, the time-dependent response of a semicrystalline polymer at isothermal uniaxial loading with small strains is determined by Eqs. (2), (18) and (29). For a standard relaxation test with the longitudinal strain ϵ^0 ,

$$\epsilon(t) = \begin{cases} 0, & t < 0, \\ \epsilon^0, & t \geq 0, \end{cases}$$

these equations imply that

$$\sigma(t, \epsilon^0) = C_1(\epsilon^0) - C_2(\epsilon^0) \int_0^\infty p(\omega) \left[1 - \exp(-\Gamma_a(\epsilon^0) \exp(-\omega)t) \right] d\omega, \quad (30)$$

where ϵ_u^0 is the strain induced by sliding of junctions and

$$C_1(\epsilon^0) = E(\epsilon^0 - \epsilon_u^0), \quad C_2(\epsilon^0) = E(\epsilon^0 - \epsilon_u^0) \kappa_a(\epsilon^0). \quad (31)$$

To fit experimental data, we adopt the random energy model [48] with

$$p(\omega) = p_0 \exp\left[-\frac{(\omega - \Omega)^2}{2\Sigma^2}\right], \quad \omega \geq 0, \quad p(\omega) = 0, \quad \omega < 0, \quad (32)$$

where Ω and Σ are adjustable parameters, and the pre-factor p_0 is determined by the condition

$$\int_0^\infty p(\omega) d\omega = 1. \quad (33)$$

Given a strain ϵ^0 , Eqs. (30) and (32) are determined by 5 material constants:

1. an analog of the average potential energy for rearrangement of strands Ω ,
2. an analog of the standard deviation for distribution of potential energies Σ ,
3. the attempt rate for separation of strands from temporary junctions in active MRs Γ_a ,
4. the coefficients C_1 and C_2 .

Our aim is to determine these parameters by fitting experimental data depicted in Figures 3 to 11.

5 Fitting of observations

We begin with matching relaxation curves for specimens not subjected to thermal treatment. First, we approximate experimental data measured at the strain $\epsilon_2 = 0.04$. This strain is chosen because it is located substantially below the yield point, on the one hand, and the testing machine ensures high accuracy of control of the strain level in the relaxation mode, on the other.

Because the rate of rearrangement, Γ_a , and the average potential energy, Ω , are mutually dependent [according to Eqs. (30) and (32), the growth of Ω results in an increase in Γ_a], we set $\Gamma_a = 1$ s and approximate the relaxation curve by using 4 experimental constants: Ω , Σ , C_1 and C_2 . To find these quantities, we fix the intervals $[0, \Omega_{\max}]$ and $[0, \Sigma_{\max}]$, where the “best-fit” parameters Ω and Σ are assumed to be located, and divide these intervals into J subintervals by the points $\Omega_i = i\Delta_\Omega$ and $\Sigma_j = j\Delta_\Sigma$ ($i, j = 1, \dots, J$) with $\Delta_\Omega = \Omega_{\max}/J$, $\Delta_\Sigma = \Sigma_{\max}/J$. For any pair, $\{\Omega_i, \Sigma_j\}$, we evaluate the integral in Eq. (30) numerically (by Simpson’s method with 200 points and the step $\Delta_\omega = 0.1$). The

pre-factor p_0 is determined by Eq. (33). The coefficients $C_1 = C_1(i, j)$ and $C_2 = C_2(i, j)$ are found by the least-squares method from the condition of minimum of the function

$$\mathcal{J}(i, j) = \sum_{t_m} [\sigma_{\text{exp}}(t_m) - \sigma_{\text{num}}(t_m)]^2, \quad (34)$$

where the sum is calculated over all experimental points t_m . The stress σ_{exp} in Eq. (34) is measured in the relaxation test, whereas the stress σ_{num} is given by Eq. (30). The “best-fit” parameters Ω and Σ minimize the function \mathcal{J} on the set $\{\Omega_i, \Sigma_j \mid (i, j) = 1, \dots, J\}$. After determining the “best-fit” values, Ω_i and Σ_j , we repeat this procedure for the new intervals $[\Omega_{i-1}, \Omega_{i+1}]$ and $[\Sigma_{j-1}, \Sigma_{j+1}]$ to ensure good accuracy of fitting. Figure 4 demonstrates fair agreement between the experimental data and the results of numerical simulation with $\Omega = 4.29$ and $\Sigma = 4.34$.

To approximate relaxation curves at other strains, ϵ_k , we fix the constants Ω and Σ found by matching observations at ϵ_2 and fit every relaxation curve by using 3 adjustable parameters: Γ_a , C_1 and C_2 . These quantities are determined by using a procedure similar to that employed in the approximation of the relaxation curve at ϵ_2 . We fix the interval $[0, \Gamma_{\text{max}}]$, where the “best-fit” attempt rate Γ_a is supposed to be located, and divide this interval into J subintervals by the points $\Gamma_i = i\Delta_\Gamma$ ($i = 1, \dots, J$) with $\Delta_\Gamma = \Gamma_{\text{max}}/J$. For any Γ_i , we calculate the integral in Eq. (30) numerically and calculate the coefficients $C_1 = C_1(i)$ and $C_2 = C_2(i)$ by the least-squares method from the condition of minimum for function (34). The “best-fit” attempt rate minimizes the function \mathcal{J} on the set $\{\Gamma_i \mid (i = 1, \dots, J)\}$. When this “best-fit” value, Γ_i , is found, the procedure is repeated for the new interval $[\Gamma_{i-1}, \Gamma_{i+1}]$ to ensure an acceptable accuracy of fitting. Figures 3 to 11 show good agreement between the observations and the results of numerical analysis.

The above algorithm of fitting is repeated to approximate the relaxation curves for specimens annealed for 4 and 24 hours. The “best-fit” parameters Ω and Σ read 5.70 and 4.88 for samples annealed for 4 h and 5.19 and 3.80 for specimens annealed for 24 h, respectively.

For a quasi-Gaussian distribution function (32), the parameters Ω and Σ do not coincide with the average potential energy for detachment of active strands, Ω_0 , and the standard deviation of potential energies for separation of strands from the network, Σ_0 . The latter quantities read

$$\Omega_0 = \int_0^\infty \omega p(\omega) d\omega, \quad \Sigma_0 = \left[\int_0^\infty (\omega - \Omega_0)^2 d\omega \right]^{\frac{1}{2}}. \quad (35)$$

The dimensionless parameters Ω_0 , Σ_0 and $\xi = \Sigma_0/\Omega_0$ given by Eq. (35) are listed in Table 1 which shows that the width of the quasi-Gaussian distribution (characterized by the ratio ξ) monotonically decreases with annealing time (however, changes in ξ are rather weak).

For any longitudinal strain ϵ_k , the attempt rate, $\Gamma_a(\epsilon_k)$, is determined by matching an appropriate relaxation curve. The fraction of active MRs, $\kappa_a(\epsilon_k)$, is found from Eq. (31),

$$\kappa_a(\epsilon_k) = \frac{C_2(\epsilon_k)}{C_1(\epsilon_k)}.$$

These quantities are plotted versus strain ϵ in Figures 12 and 13. The experimental data are approximated by the phenomenological equations

$$\log \Gamma_a = \gamma_0 + \gamma_1 \epsilon, \quad \kappa_a = k_0 + k_1 \epsilon, \quad (36)$$

where the coefficients γ_i and k_i are found by the least-squares method. Figures 12 and 13 reveal that the viscoelastic behavior of specimens not subjected to thermal treatment is rheologically simple in the sense that the quantities Γ_a and κ_a in Eq. (30) are independent of strain. On the contrary, annealed samples demonstrate the time-dependent behavior that is strongly affected by loading: with an increase in strain, the attempt rate, Γ_a , exponentially decreases and the fraction of active MRs, κ_a , linearly grows.

According to Figure 12, the attempt rate, Γ_a , is strain-independent for non-annealed specimens (however, the scatter of the experimental data is rather large). A detailed analysis of relaxation curves for non-annealed samples [49] shows that the attempt rate increases in the range of strains from $\epsilon = 0.005$ to $\epsilon = 0.02$ and remains constant at $\epsilon \geq 0.02$. This implies that the free-volume concept [44, 45, 46] is valid for isotactic polypropylene, but the area of its applicability is confined to relatively small deformations far below the yield strain.

6 Discussion

Several approaches were recently proposed to the description of the viscoplastic behavior of isotactic polypropylene in the vicinity of the yield point. Aboulfaraj et al. [27] presumed that plastic slip mechanisms had noticeably different features in α and β structures. Karger-Kocsis and Varga [50] and Karger-Kocsis et al. [51] explained toughening of iPP by mechanically-induced $\beta \rightarrow \alpha$ transformation of crystallites. Raab et al. [52] associated the difference in the response of α and β spherulites with different types of chain folding in lamellae.

Three substantial shortcomings of these concepts should be mentioned:

1. they are based on some hypotheses about the difference in the mechanical behavior of α and β crystallites which have not yet been confirmed experimentally,
2. these models imply that changes in the stress-strain diagrams of iPP at annealing are associated with an increase in the content of β -polymorph, which contradicts to WAXS (wide angle X-ray scattering) diagrams obtained by Iijima and Strobl [26],
3. these approaches do not expound a pronounced decrease in the relaxation rate with strain for annealed samples exhibited in Figure 12.

The results presented in Figures 1, 12 and 13 may be explained in terms of the growth of heterogeneity in the distribution of lamellar strength notwithstanding whether the fraction of β spherulites increases at annealing.

An increase in the low-temperature shoulder of the DSC traces depicted in Figure 1 (at a practically constant enthalpy of melting) means that the content of “weak” crystalline lamellae (that melt at relatively low temperatures) noticeably grows. These “weak” lamellae may be associated with subsidiary lamellae in α spherulites.

Using a thermo-mechanical analogy, one can speculate that the growth of the fraction of thermally weak lamellae at annealing is tantamount to an increase in the concentration of lamellae which can be easily fragmented under stretching. The latter reflects an increase in structural disorder of α crystallites at annealing far below the melting point observed as substantial variations in the relative intensity of Bragg reflections [53].

On the other hand, annealing of isotactic polypropylene induces thickening of radial lamellae, which results in the growth of elastic moduli of the polymer. This implies that at relatively small strains ($\epsilon < 0.02$ to 0.04 , when fragmentation of lamellae does not occur), annealing of iPP leads to an increase in the longitudinal stress (which is demonstrated in Figure 2). At higher strains, the coarse slip starts in weak lamellae of specimens annealed for 24 h (which are less homogeneous than those annealed for 4 h), whereas no lamellar fragmentation takes place in samples annealed for 4 h. As a consequence, the stress-strain curve 2 is located higher than the curve 3 in Figure 2. With an increase in strain, lamellar fragmentation occurs in both specimens, which implies that the stress-strain curves for annealed specimens practically coincide at strains exceeding the yield point $\epsilon_y = 0.13$.

Further increase in strain in the post-yield region results in total fragmentation of lamellae that can be broken at a given stress intensity in specimens not subjected to thermal treatment. Because homogeneous (along a specimen) crystal slip becomes impossible, spatial heterogeneity in the distribution of stresses arises at the macro-level, which leads to necking of the specimens at $\epsilon_n = 0.18$. For the samples annealed for 4 and 24 hours, the concentration of “weak” lamellae is higher, which implies that the strains corresponding to the total fragmentation of weak lamellae and transition to the spatially heterogeneous deformation of specimens exceed that for the non-annealed material ($\epsilon_n = 0.25$ and $\epsilon_n > 0.30$, respectively).

Noticeable fragmentation of lamellae in spherulites implies that some amorphous regions are released (whose deformation was previously screened by surrounding lamellae in non-broken crystallites), which results in an increase in the fraction of active MRs, κ_a , with strain. This release of restricted amorphous phase is substantially less pronounced in the specimens not subjected to thermal treatment (curve 1 in Figure 13) compared with the annealed specimens (curves 2 and 3 in Figure 13). Three features of the curves depicted in Figure 13 are worth to be mentioned:

1. At small strains (less than 0.04), the concentration of active MRs monotonically decreases with annealing time. This phenomenon may be attributed to an increase in the fraction of amorphous regions whose mobility is restricted by surrounding lamellae at annealing (driven by development of subsidiary lamellae).
2. The content of active meso-domains linearly grows with strain in annealed specimens with the rate that is practically independent of the annealing time. This may be explained by changes in the micro-structure of spherulites at annealing: although the rate of lamellar fragmentation is assumed to be higher in iPP annealed for 24 h, the amount of amorphous phase released at any fragmentation act is smaller than in iPP annealed for 4 h.
3. Curves 2 and 3 intersect curve 1 in the region between $\epsilon = 0.08$ and $\epsilon = 0.12$, i.e., in the close vicinity of the yield point for non-annealed specimens (see Figure 2).

With reference to Coulon et al. [29] and Raab et al. [52], we suppose that under stretching lamellae are fragmented into small aligned blocks that serve as extra physical cross-links in amorphous meso-domains. According to the concept of transient networks [42], an increase in the concentration of permanent cross-links results in a decrease in the net rate of rearrangement. This rate is characterized in the model by the attempt rate, Γ_a , which is considered as an average (over MRs) rate of detachment of active strands from their junctions. This conclusion is fairly well confirmed by the results depicted in Figure 12: the attempt rate is practically independent of strain for the specimens not subjected to thermal pre-treatment, and Γ_a exponentially decreases with strain for the annealed samples. Despite apparent similarity in the slopes of curves 2 and 3 in Figure 12, it is rather difficult to assert that the kinetics of the strain-induced decrease in the attempt rate is independent of annealing time because of the large scatter of data for the specimens annealed for 24 h. It is worth noting that the attempt rates were determined in Section 5 from the condition $\Gamma_a = 1$ s at $\epsilon = 0.04$, which implies that their values cannot be directly compared for specimens annealed for different amounts of time (because these samples have different distributions of potential energies for separation of active strands from temporary nodes, see Table 1).

7 Concluding remarks

Constitutive equations have been derived for the time-dependent behavior of semicrystalline polymers at isothermal loading with small strains. A mean-field approach is employed to develop stress-strain relations: a complicated micro-structure of isotactic polypropylene is replaced by an equivalent transient network of macromolecules bridged by junctions (physical cross-links, entanglements and crystalline lamellae). The network is assumed to be strongly inhomogeneous, and it is thought of as an ensemble of meso-regions with various potential energies for separation of strands from temporary nodes.

The viscoelastic response of a semicrystalline polymer is ascribed to separation of active strands from temporary junctions and merging of dangling strands to the network in active meso-domains. Rearrangement of strands is modelled as a thermo-mechanically activated process whose rate is given by the Eyring equation with a strain-dependent attempt rate.

The viscoplastic response is described by slippage of junctions with respect to their positions in the bulk material. The rate of sliding is assumed to be proportional to the macro-stress in a specimen.

Three series of tensile relaxation tests have been performed on isotactic polypropylene at ambient temperature. In the first series, injection-molded samples are used without thermal pre-treatment. In the second series, the samples are annealed at 130 °C for 4 h, and in the last series, the specimens are annealed for 24 h at the same temperature. Adjustable parameters in the stress-strain relations are found by fitting observations in the range of strains from 0.02 to 0.18. The following conclusions are drawn from the analysis of experimental data:

1. The relaxation spectrum of iPP (which is determined by the distribution function, $p(\omega)$, for potential energies of detachment of active strands from their junctions) is

not affected by mechanical factors, but is altered at annealing.

2. The attempt rate, Γ_a , for separation of active strands from temporary nodes is practically independent of strain for specimens not subjected to thermal treatment, and it exponentially decreases with strain for annealed samples.
3. The relaxation strength (which is characterized by the content of active meso-regions κ_a) is independent of strain for non-annealed specimens, and it linearly increases with strain for annealed samples.

These findings are qualitatively explained based on the hypothesis that the distribution of strengths of crystalline lamellae in iPP is noticeably broadened at annealing, which results not only in thickening of lamellae, but also in the growth of “weak” (subsidiary) lamellae that are easily fragmented either by heating or by mechanical loading. DSC measurements provide some confirmation for this assumption.

References

- [1] Kalay G and Bevis MJ 1997 *J. Polym. Sci. B: Polym. Phys.* **35** 241–263, 265–291
- [2] Ward IM and Wolfe JM 1966 *J. Mech. Phys. Solids* **14** 131–140
- [3] Ward IM and Hadley DW 1993 *An Introduction to the Mechanical Properties of Solid Polymers* (New York: Wiley)
- [4] Smart J and Williams JG 1972 *J. Mech. Phys. Solids* **20** 313–324
- [5] Ariyama T 1993a *Polym. Eng. Sci.* **33** 18–26
- [6] Ariyama T 1993b *Polym. Eng. Sci.* **33** 1494–1499
- [7] Ariyama T 1996 *J. Mater. Sci.* **31** 4127–4131
- [8] Ariyama T, Mori Y, and Kaneko K 1997 *Polym. Eng. Sci.* **37** 81–90
- [9] Wortmann F-J and Schulz KV 1994 *Polymer* **35** 2108–2117
- [10] Wortmann F-J and K.V. Schulz KV 1995 *Polymer* **36** 2363–2369
- [11] Ibhaddon AO 1996 *J. Appl. Polym. Sci.* **62** 1843–1846
- [12] Tomlins PE *Polymer* **37** 3907–3913
- [13] Dutta NK and Edward GH 1997 *J. Appl. Polym. Sci.* **66** 1101–1115
- [14] Read BE and Tomlins PE 1997a *Polymer* **38** 4617–4628
- [15] Read BE and Tomlins PE 1997b *Polym. Eng. Sci.* **37** 1572–1581
- [16] Tomlins PE and Read BE 1998 *Polymer* **39** 355–367
- [17] Struik LCE 1978 *Physical Aging in Amorphous Polymers and Other Materials* (Amsterdam: Elsevier).
- [18] Struik LCE 1987 *Polymer* **28** 1521–1535
- [19] Chai CK and McCrum NG 1980 *Polymer* **21** 706–718
- [20] Andreassen E 1999 *Polymer* **40** 3909–3918
- [21] Seguela R, Staniek E, Escaig B, and Fillon B 1999 *J. Appl. Polym. Sci.* **71** 1873–1885
- [22] Bicerano J 1998 *J. Macromol. Sci. C: Rev. Macromol. Chem. Phys.* **38** 391–480
- [23] Labour T, Gauthier C, Seguela R, Vigier G, Bomal Y, and Orange G 2001 *Polymer* **42** 7127–7135
- [24] Labour T, Vigier G, Seguela R, Gauthier C, Orange G, and Bomal Y 2002 *J. Polym. Sci. B: Polym. Phys.* **40** 31–42

- [25] Alamo RG, Kim M-H, Galante MJ, Isasi JR, and Mandelkern L 1999 *Macromolecules* **32** 4050–4064
- [26] Iijima M and Strobl G 2000 *Macromolecules* **33** 5204–5214
- [27] Aboulfaraj M, G’Sell C, Ulrich B, and Dahoun A 1995 *Polymer* **36** 731–742
- [28] Labour T, Ferry L, Gauthier C, Hajji P, and Vigier G 1999 *J. Appl. Polym. Sci.* **74** 195–200
- [29] Coulon G, Castelein G, and G’Sell C 1998 *Polymer* **40** 95–110
- [30] Maiti P, Hikosaka M, Yamada K, Toda A, and Gu F 2000 *Macromolecules* **33** 9069–9075
- [31] Androsch R and Wunderlich B 2001 *Macromolecules* **34** 5950–5960
- [32] Zhang XC, Butler MF, and Cameron RE 1999 *Polym. Int.* **48** 1173–1178
- [33] Bergstrom JS, Kurtz SM, Rimnac CM, and Edidin AA 2002 *Biomaterials* **23** at press
- [34] Nitta K-H and Takayanagi M 1999 *J. Polym. Sci. B: Polym. Phys.* **37** 357–368
- [35] Nitta K-H and Takayanagi M 2000 *J. Polym. Sci. B: Polym. Phys.* **38** 1037–1044
- [36] Meyer RW and Pruitt LA 2001 *Polymer* **42** 5293–5306
- [37] Sweeney J and Ward IM 1996 *J. Mech. Phys. Solids* **44** 1033–1049
- [38] Boyce MC, Socrate S, and Llana PG 2000 *Polymer* **41** 2183–2201
- [39] Green MS and Tobolsky AV 1946 *J. Chem. Phys.* **14** 80–92
- [40] Yamamoto M 1956 *J. Phys. Soc. Japan* **11** 413–421
- [41] Lodge AS 1968 *Rheol. Acta* **7** 379–392
- [42] Tanaka F and Edwards SF 1992 *Macromolecules* **25** 1516–1523
- [43] Krausz AS and Eyring H 1975 *Deformation Kinetics* (New York: Wiley)
- [44] Knauss WG and Emri IJ 1987 *Polym. Eng. Sci.* **27** 86–100
- [45] Losi GU and Knauss WG 1992 *Polym. Eng. Sci.* **32** 542–557
- [46] O’Dowd NP and Knauss WG 1995 *J. Mech. Phys. Solids* **43** 771–792
- [47] Wunderlich B 1980 *Macromolecular Physics*. Vol. 3, *Crystal Melting* (New York: Academic)
- [48] Dyre JC 1995 *Phys. Rev. B* **51** 12276–12294
- [49] Drozdov AD and Christiansen JdeC 2002 Preprint cond-mat/0201117

- [50] Karger-Kocsis J and Varga J 1996 *J. Appl. Polym. Sci.* **62** 291–300
- [51] Karger-Kocsis J, Varga J, and Ehrenstein GW 1997 *J. Appl. Polym. Sci.* **64** 2057–2066
- [52] Raab M, Kotek J, Baldrian J, and Grellmann W 1998 *J. Appl. Polym. Sci.* **69** 2255–2259
- [53] Auriemma F, Ruiz de Ballesteros O, de Rosa C, and Corradini P 2000 *Macromolecules* **33** 8764–8774

List of figures

Figure 1: DSC melting curves for a non-annealed specimen (unfilled circles), a specimen annealed for 4 h (filled circles) and a specimen annealed for 24 h (triangles). Symbols: experimental data

Figure 2: The longitudinal stress σ MPa versus strain ϵ in tensile tests with the cross-head speed 5 mm/min. Symbols: experimental data. Unfilled circles: a virgin specimen; filled circles: a specimen annealed for 4 h; triangles: a specimen annealed for 24 h; asterisks: stresses at the beginning of relaxation tests at various strains

Figure 3: The longitudinal stress σ MPa versus time t s in a tensile relaxation test at $\epsilon = 0.02$. Symbols: experimental data. Solid lines: results of numerical simulation. Curve 1: a virgin specimen; curve 2: a specimen annealed for 4 h; curve 3: a specimen annealed for 24 h

Figure 4: The longitudinal stress σ MPa versus time t s in a tensile relaxation test at $\epsilon = 0.04$. Symbols: experimental data. Solid lines: results of numerical simulation. Curve 1: a virgin specimen; curve 2: a specimen annealed for 4 h; curve 3: a specimen annealed for 24 h

Figure 5: The longitudinal stress σ MPa versus time t s in a tensile relaxation test at $\epsilon = 0.06$. Symbols: experimental data. Solid lines: results of numerical simulation. Curve 1: a virgin specimen; curve 2: a specimen annealed for 4 h; curve 3: a specimen annealed for 24 h

Figure 6: The longitudinal stress σ MPa versus time t s in a tensile relaxation test at $\epsilon = 0.08$. Symbols: experimental data. Solid lines: results of numerical simulation. Curve 1: a virgin specimen; curve 2: a specimen annealed for 4 h; curve 3: a specimen annealed for 24 h

Figure 7: The longitudinal stress σ MPa versus time t s in a tensile relaxation test at $\epsilon = 0.10$. Symbols: experimental data. Solid lines: results of numerical simulation. Curve 1: a virgin specimen; curve 2: a specimen annealed for 4 h; curve 3: a specimen annealed for 24 h

Figure 8: The longitudinal stress σ MPa versus time t s in a tensile relaxation test at $\epsilon = 0.12$. Symbols: experimental data. Solid lines: results of numerical simulation. Curve 1: a virgin specimen; curve 2: a specimen annealed for 4 h; curve 3: a specimen annealed for 24 h

Figure 9: The longitudinal stress σ MPa versus time t s in a tensile relaxation test at $\epsilon = 0.14$. Symbols: experimental data. Solid lines: results of numerical simulation. Curve 1: a virgin specimen; curve 2: a specimen annealed for 4 h; curve 3: a specimen annealed for 24 h

Figure 10: The longitudinal stress σ MPa versus time t s in a tensile relaxation test at $\epsilon = 0.16$. Symbols: experimental data. Solid lines: results of numerical simulation. Curve 1: a virgin specimen; curve 2: a specimen annealed for 4 h; curve 3: a specimen

annealed for 24 h

Figure 11: The longitudinal stress σ MPa versus time t s in a tensile relaxation test at $\epsilon = 0.18$. Symbols: experimental data. Solid lines: results of numerical simulation. Curve 2: a specimen annealed for 4 h; curve 3: a specimen annealed for 24 h

Figure 12: The attempt rate Γ_a s⁻¹ versus strain ϵ in tensile relaxation tests. Symbols: treatment of observations. Unfilled circles: virgin specimens; filled circles: specimens annealed for 4 h; triangles: specimens annealed for 24 h. Solid lines: approximation of the experimental data by Eq. (36). Curve 1: $\gamma_0 = -0.15$, $\gamma_1 = -0.08$; curve 2: $\gamma_0 = 0.12$, $\gamma_1 = -2.91$; curve 3: $\gamma_0 = 0.05$, $\gamma_1 = -2.99$

Figure 13: The concentration of active MRs κ_a versus strain ϵ in tensile relaxation tests. Symbols: treatment of observations. Unfilled circles: virgin specimens; filled circles: specimens annealed for 4 h; triangles: specimens annealed for 24 h. Solid lines: approximation of the experimental data by Eq. (36). Curve 1: $k_0 = 0.57$, $k_1 = 0.01$; curve 2: $k_0 = 0.47$, $k_1 = 1.55$; curve 3: $k_0 = 0.39$, $k_1 = 1.49$

Table 1: Adjustable parameters Ω_0 , Σ_0 and ξ at various annealing times t_a h

t_a	Ω_0	Σ_0	ξ
0	5.49	3.36	0.61
4	6.58	3.74	0.57
24	5.80	3.22	0.55

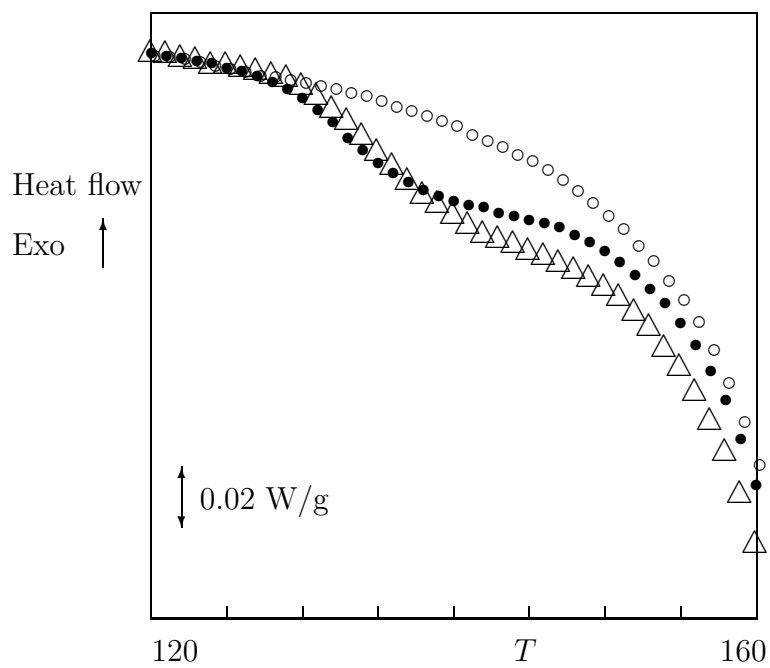


Figure 1:

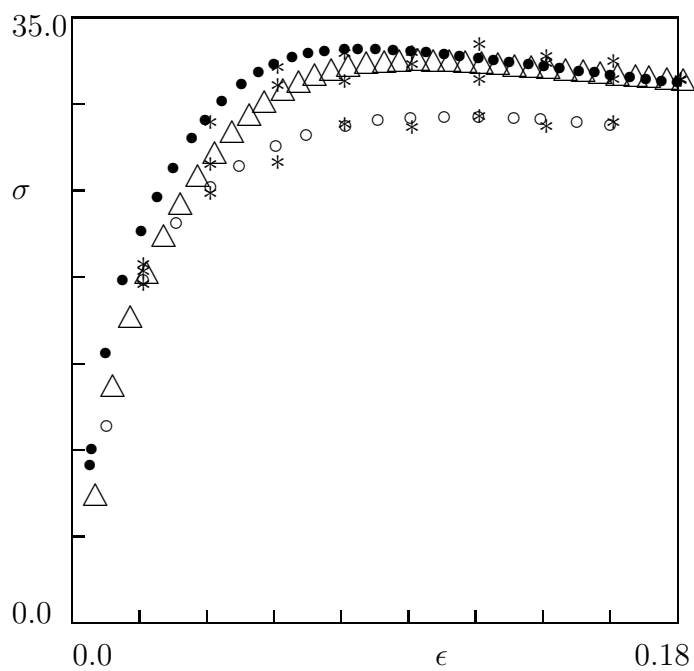


Figure 2:

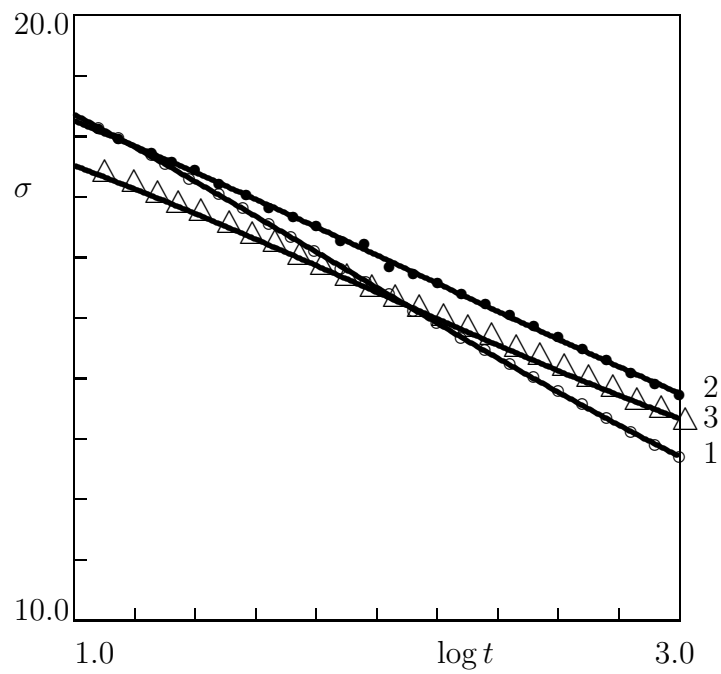


Figure 3:

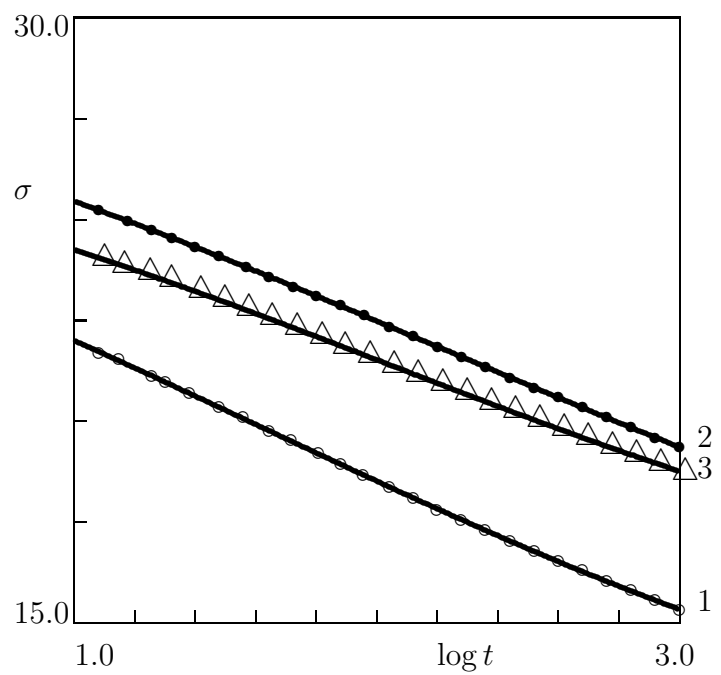


Figure 4:

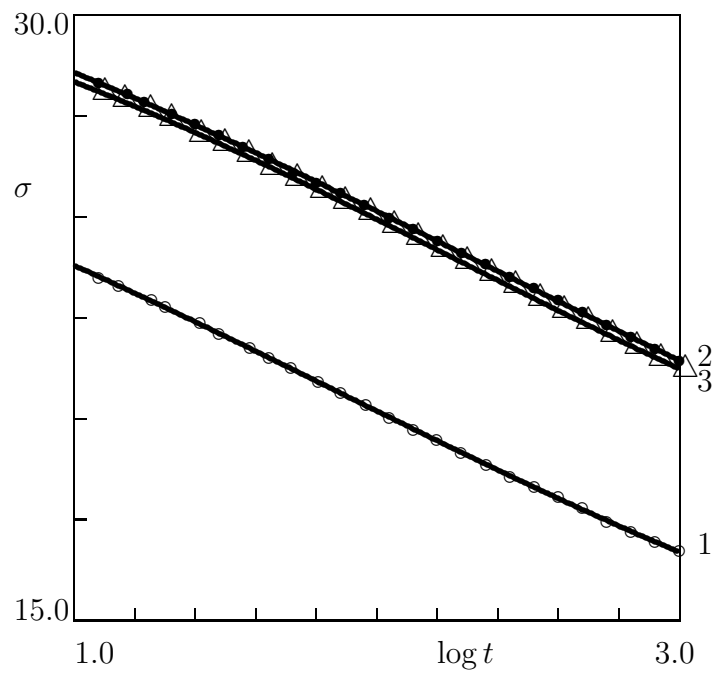


Figure 5:

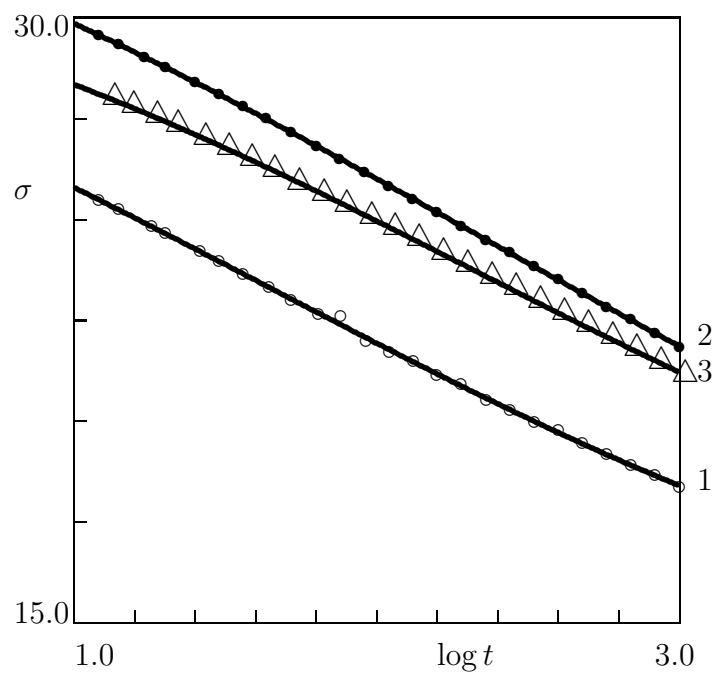


Figure 6:

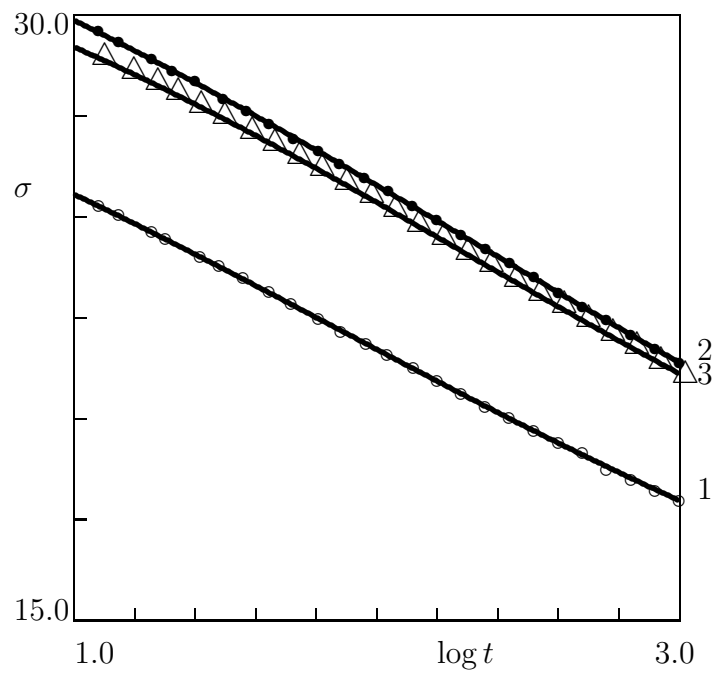


Figure 7:

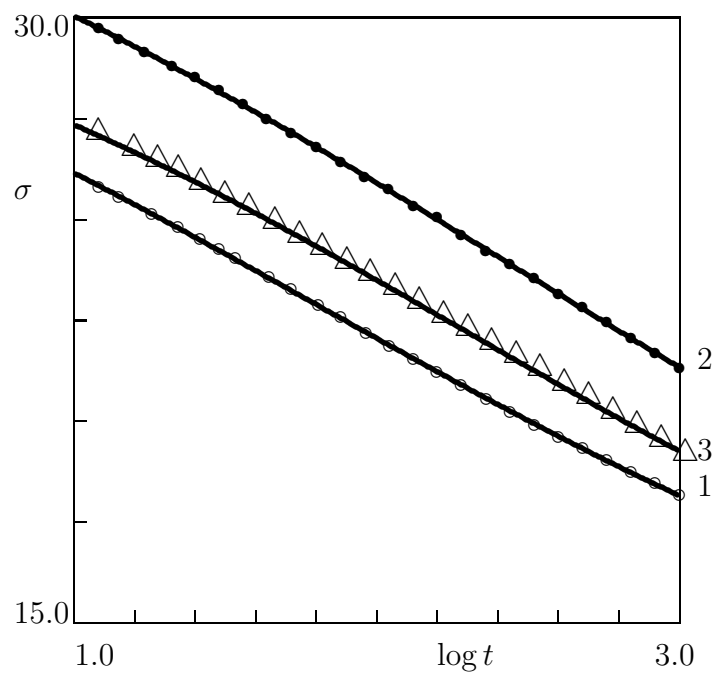


Figure 8:

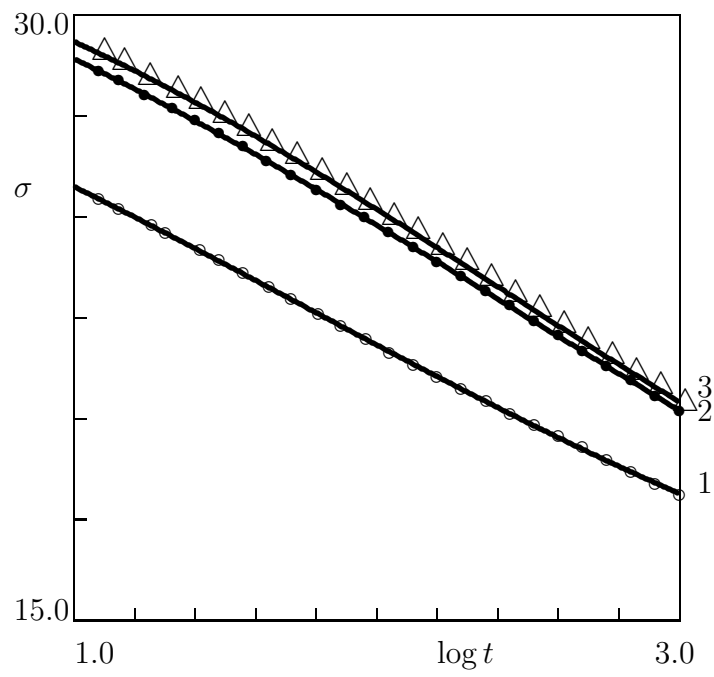


Figure 9:

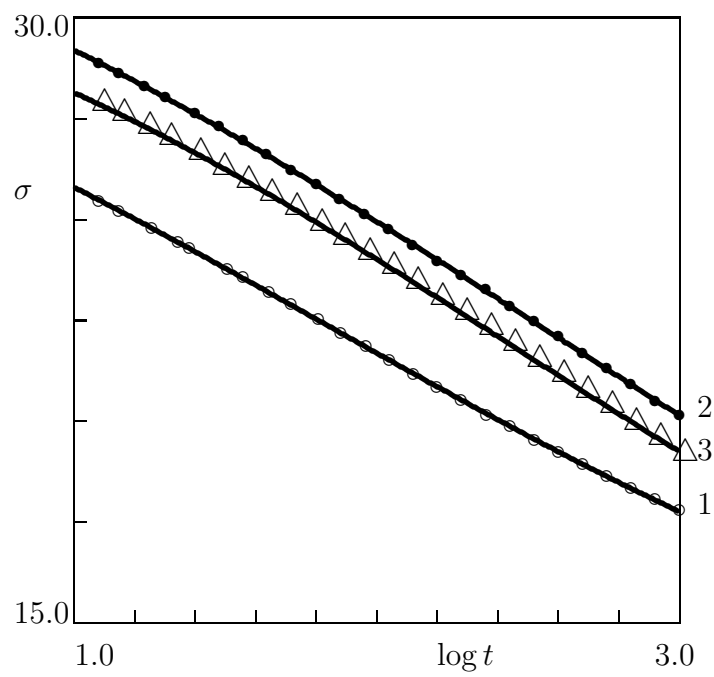


Figure 10:

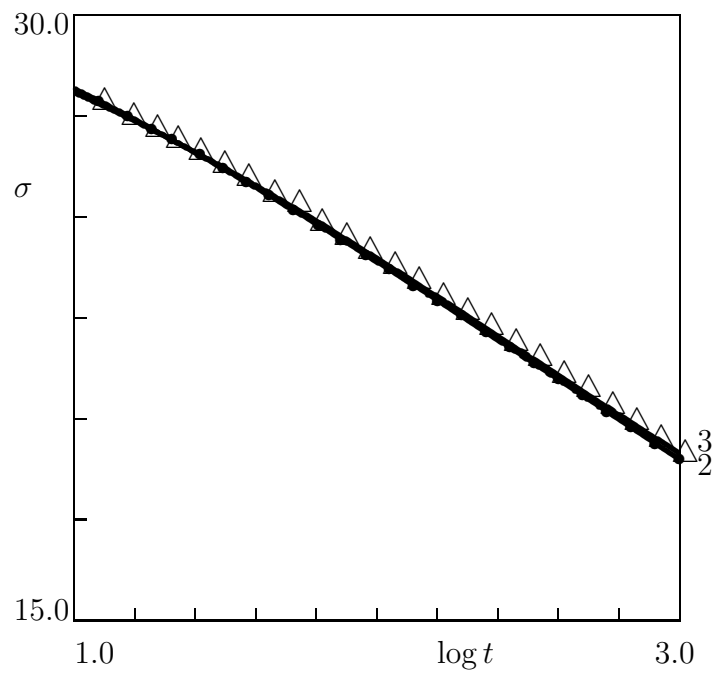


Figure 11:

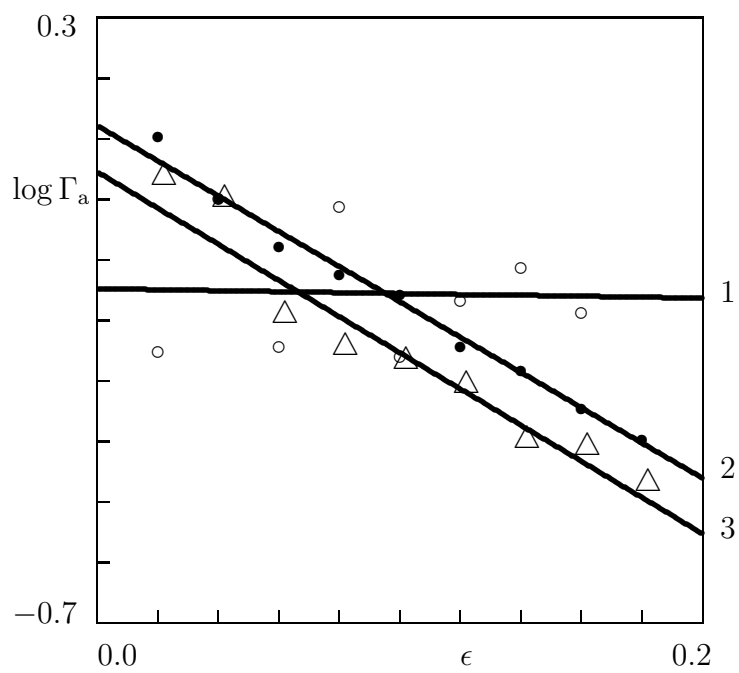


Figure 12:

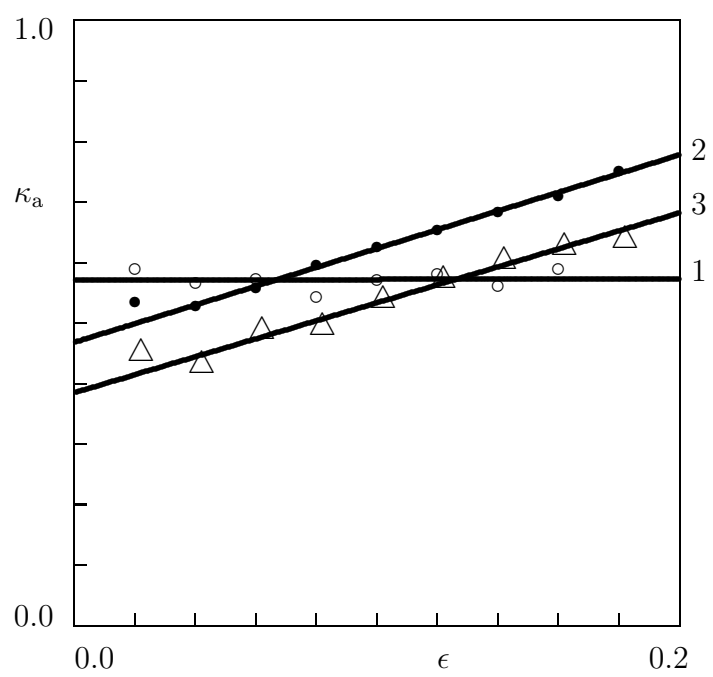


Figure 13: